Supplementary information for

Thermal Stabilities of Mn-based Active Materials in Combination with the Ceramic Electrolyte LATP for ASSB Bulk Cathodes

Matthias Rumpel,[a] Felix Nagler,[a] Lavinia Appold,[a] Werner Stracke,[a] Andreas Flegler,[a] Oliver Clemens[b] and Gerhard Sextl[a]

Fraunhofer Institute for Silicate Research ISC, Neunerplatz 2, 97082 Wuerzburg, Germany[a]

University Stuttgart, Institute for Material Sciences, Chemical Materials Synthesis, Heisenbergstraße 3, 70569 Stuttgart, Germany[b]

Fig. S1: Starting Powders

The particle size distributions of all powders are comparable, which is important for the following HT-XRD and DSC-TG measurements, since a homogeneous mixture of the powders results in a maximum amount of contacts between the materials. Consequently, the signal of the reactions and mixed phase formation is more accurate.

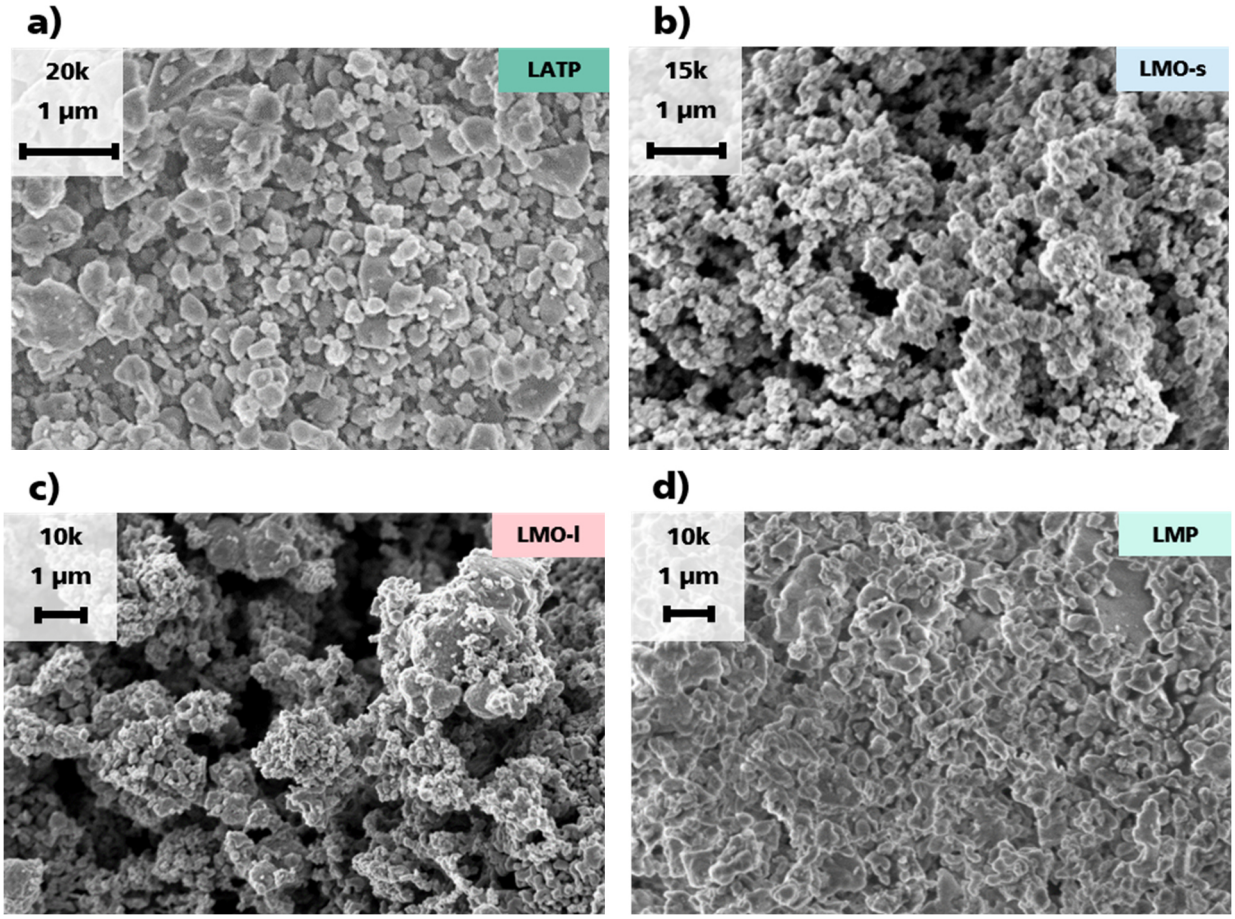

Fig S1 SEM images of the starting powders: a) LATP, b) LMO-s, c) LMO-l and d) LMP. Particle size distributions are comparable and particle sizes are < 1 µm.

Fig. S2: XRD Diffractograms and Rietveld Refinement of LMO-s and LATP Powder Mixture

All starting powders are free from impurity phases (Fig. S2a). LMP, LMO-l and LATP are intrinsically thermally stable (Fig. S2b). LMO-s shows decomposition processes and mass loss starting at ca. 550 °C in argon atmosphere.

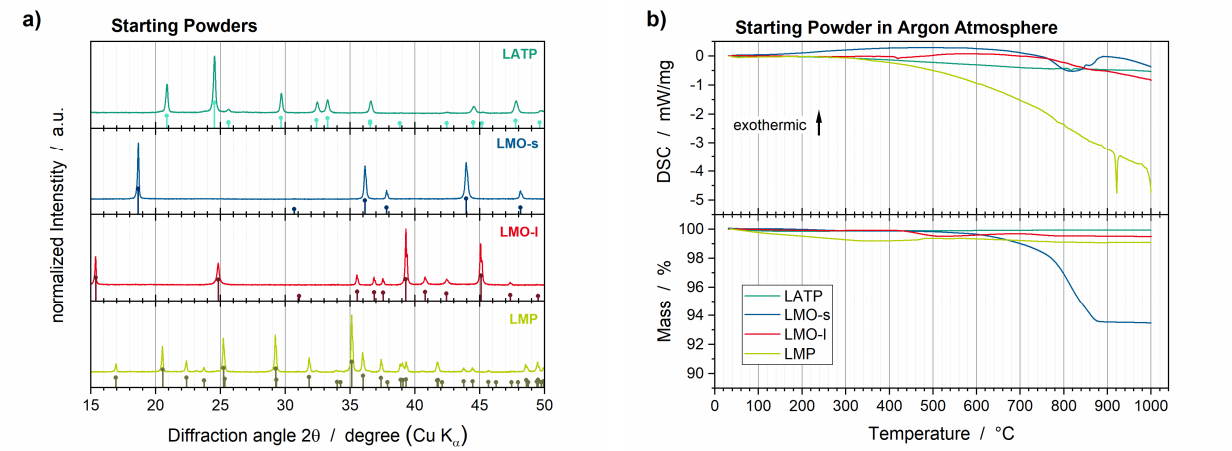

Fig S2 Characterization of starting powders LATP (dark green), LMO-s (blue), LMO-l (red) and LMP (light green): a) XRD patterns and b) DSC-TG profiles.

Table. S1: Table of References and Information about Rietveld Refinement of HT-XRD Measurements

The references used for Rietveld refinement are summarized in the following:

Phase	Space Group	ICSD Nr.	Phase	Space Group	ICSD Nr.
$LiMn_2O_4$ (LMO-s)	$Fd\bar{3}m$	50427			
$LiMnO_2$ (LMO-l)	$C/2m$	82993	Mn_3O_4	$I4_1/amd$	10925
$LiMnPO_4$ (LMP)	$Pnma$	25834	Mn_2O_3	$Ia\bar{3}$	9091
LATP	$R\bar{3}c$	95979			
Li_3PO_4	$Pnma$	79427	$MnTiO_3$	$R\bar{3}$	184649
$LiTiOPO_4$	$Pnma$	153522	$Li(Mn,Ti)_2O_4$	$P4_332$	238491
TiO_2 (anatase)	$I4_1/amd$	93039	$Mn_2P_2O_7$	$C/2m$	20296
TiO_2 (rutile)	$P4_2/mnm$	167964			

A Chebyshev polynomial function of order 20 was used to fit the background; since this order is high, linearity of the background below individual reflections / reflection groups was checked individually. Due to the reaction processes occurring at a certain temperature, a compromise between signal-to-noise ratio and measurement duration had to be made. With respect of this and due to the short measurement duration (15 min in order to avoid impact of significant changes during measurement due to decomposition) at each temperature step and the argon atmosphere, the background appear to be noisy due to a low signal-to-noise ratio. A PSD detector was used to obtain optimal signals despite short measurement times. To guarantee most accurate Rietveld refinement and phase fractions, only lattice parameter and crystallite sizes were refined by setting physically reasonable minima and maxima for the refinement for reflection widths, by which quantification errors and run-away of parameters can be avoided. After refinement, parameters did not reach the boundaries of the limits provided. Two reflections of each phase could be detected and the fit accuracy as well as completeness of detected reflections were double-checked visually.

Fig. S3: XRD Diffractograms and Rietveld Refinement of LMO-s and LATP Powder Mixture

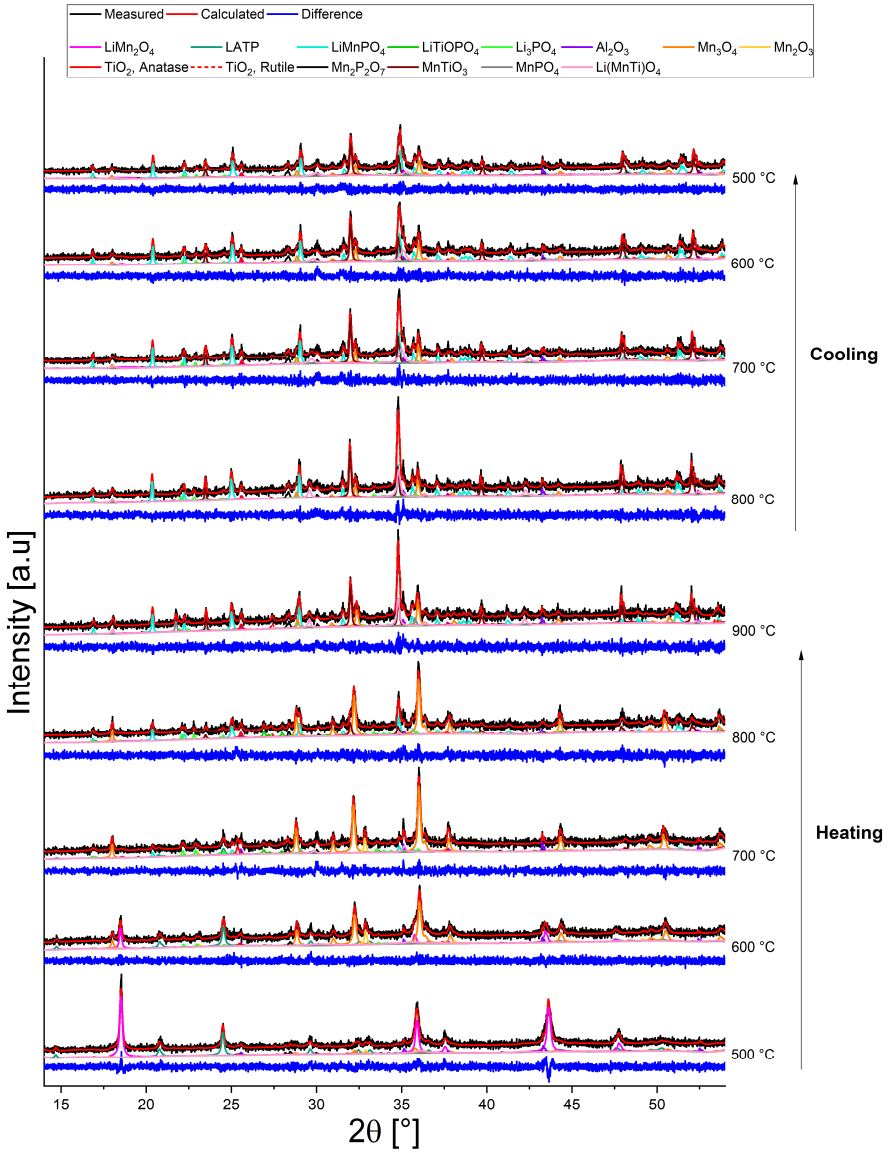

Fig. S3 Selection of the XRD diffractograms incl. Rietveld refinement of the LMO-s + LATP powder mixture at various temperatures.

Fig. S4: XRD Diffractograms and Rietveld Refinement of LMO-l and LATP Powder Mixture

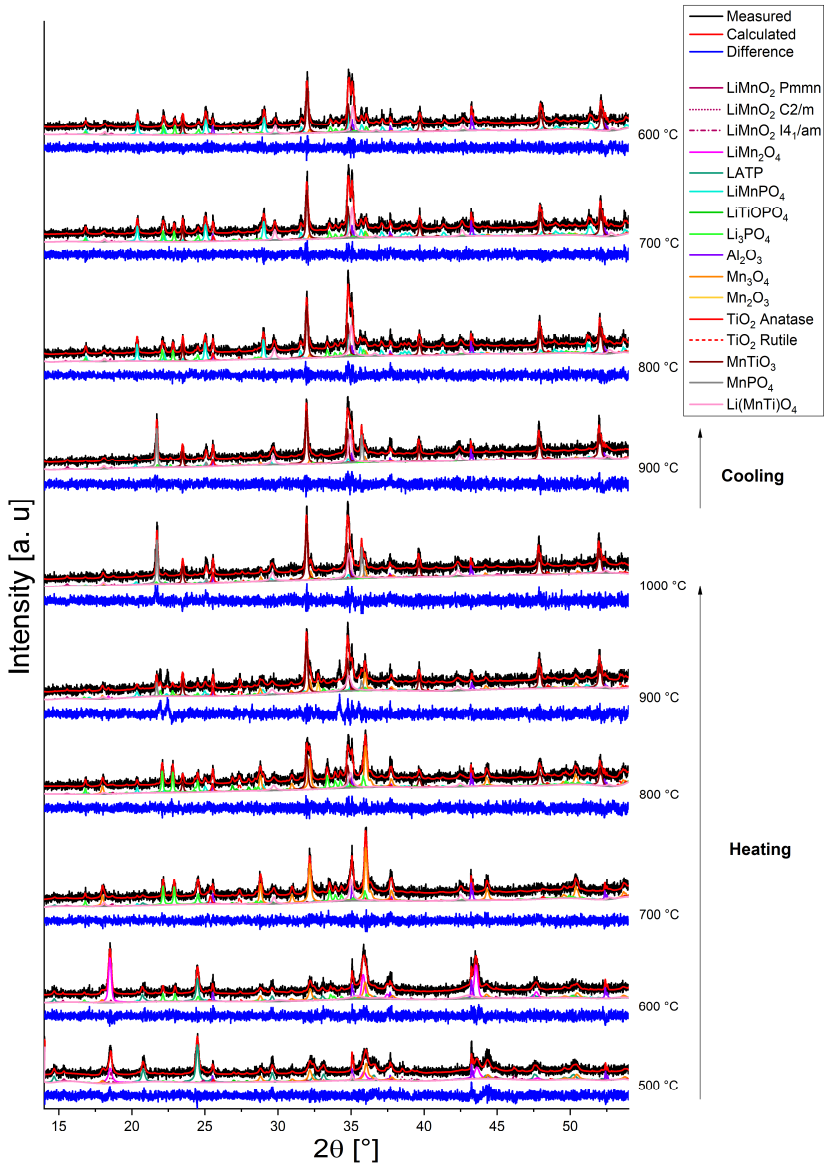

Fig. S4 Selection of the XRD diffractograms incl. Rietveld refinement of the LMO-l + LATP powder mixture at various temperatures.

Fig. S5: XRD Diffractograms and Rietveld Refinement of LMP and LATP Powder Mixture

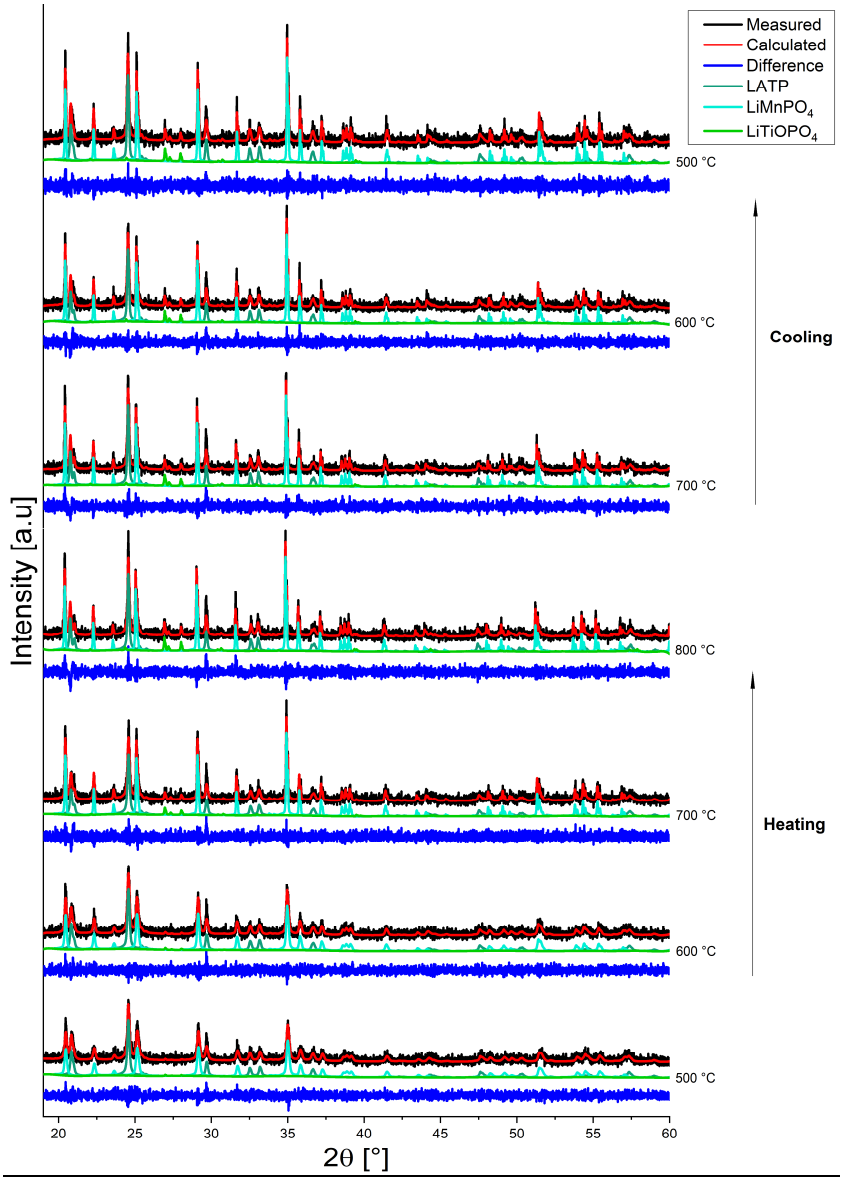

Fig. S5 Selection of the XRD diffractograms incl. Rietveld refinement of the LMP + LATP powder mixture at various temperatures.

Fig. S6: Phase Fractions of the LMP, LATP and Ag Powder Mixture

The deduced phase fractions of all XRD patterns show that the oxy-phosphate forms at 680 °C, which is similar to the LMP + LATP powder mixture. However, a deeper analysis of the Ag, LATP and LMP phase fractions cannot be done, since the Ag phase fraction shows an unusual drop of 30 wt% between 760 °C and 800 °C (Fig. S6), which corresponds to 75 mg of the 250 mg pellet. Two effects might cause the reduction of the Ag amount: the evaporation of Ag and the change in the adsorption factor A of Ag due to particle growth.

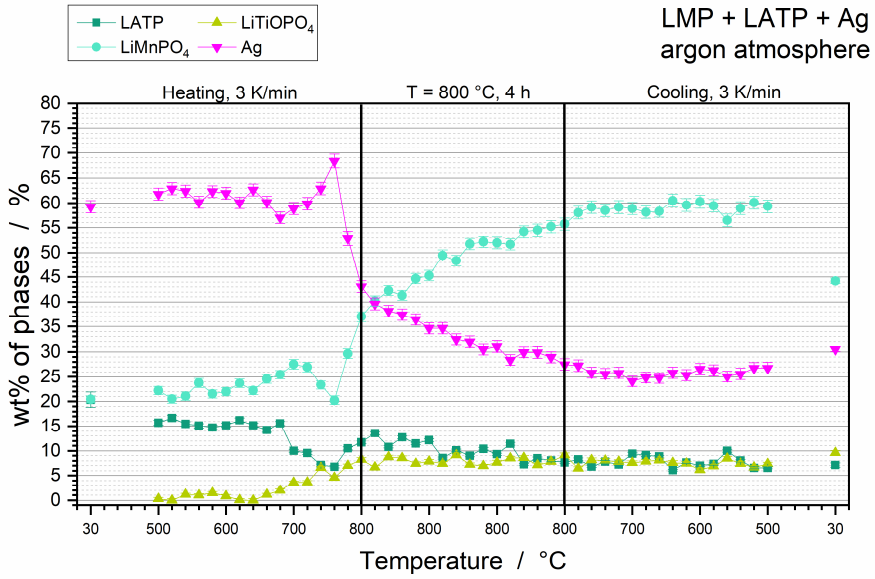

Fig. S6 Phase fractions in wt% of crystalline phases obtained by Rietveld refinement of the LMP + LATP + Ag pellets as a function of the annealing temperature. Heating up to 800 °C with 3 K/min, holding step at 800 °C for 4 h, and afterwards cooling with 3 K/min to 30 °C.

The saturation vapour pressure of solid Ag is about 6.62 x 10^{-5} Pa at 800 °C, which results in an evaporation rate of ca. 3 mg cm^{-2} h^{-1}.[1,2] As a result, ca. 12 mg cm^{-2} might theoretically evaporate during the holding step at 800 °C for 4 h. However, the calculation relates to a plane Ag surface, which is not given in our experiment, as the Ag particles are incorporated in a ternary microstructure. Additionally, the particle size of 48 nm to 78 nm results in a very high surface area, which is impossible to determine in this study. Furthermore, the particle growth to about 6 µm (Fig. 8b) decreases the surface area during the annealing process. Conclusively, an exact calculation of the evaporated Ag amount cannot be done, but the high evaporation rate indicates that the effect of Ag evaporation may have an impact on the Ag amount and finally on the HT-XRD data and phase fraction analysis. The TG curves show a low mass loss of 0.2 wt% (corresponds to 0.5 mg of a 250 mg pellet) between 800 °C and 1000 °C, which corresponds to 20 min (heating rate 10 K/min) above 800 °C. Consequently, short heating duration should be aimed for further development of the material system.

A possible error source for the Rietveld refinement might be the change in the adsorption factor A of Ag due to its dependency on the particles size d:[3]

$$A = \frac{I}{I_0} = exp(-\mu \cdot d)$$

where I_0 is the initial intensity and I is the intensity of the radiation, which is not absorbed by the material and detected from the detector. The phase specific absorption coefficient μ of Ag for Cu K_α radiation is 2289 cm^{-1}.[4] A decrease in the absorption factor means an increase in absorption of the radiation by the Ag particles. If the absorption by one phase (i.e. Ag) significantly increases, its detected scattered radiation decreases, thus the intensities in the diffractograms decreases. Additionally, it has an impact on the amount of scattering in the further phases (i.e. LMP, LATP). Consequently, the change in the absorption factor leads to wrong crystalline statistics and an error-prone quantification of the weight percentages. Applying the above equation, the absorption factor A is above 0.9 for Ag particle sizes below 1 μm, such as the starting Ag powder. After sintering at 800 °C, the SEM images reveal particle sizes of ca. 2 μm - 6 μm (Fig. 8b), which result in absorption factors between 0.6 (2 μm) and 0.2 (6 μm). Thus, the X-ray absorption by the Ag particles significantly increases with particle growth during the heat treatment, so that the maximum intensities differ with temperature and a quantitative Rietveld refinement cannot be reliably done.

In conclusion, the evaporation and particle growth of Ag during the annealing process results in an error prone Rietveld refinement and phase fraction analysis.

Fig. S7: DSC-TG incl. MS Measurement of the pure Ag powder

The pure Ag powder purchased from Nanografi® show a high mass loss between 200 °C and 400 °C due to the combustion of the carbon coating, which is necessary to prevent agglomeration after manufacturing. The MS can detect $C_xH_yO_z$ speciese in the mass to charge range of m/e = 40 to m/e = 87, which corresponds to the combustion of the carbon coating. The endothermic peak at 969 °C is in accordance with the melting point of 962 °C, reported in the data sheet.[5]

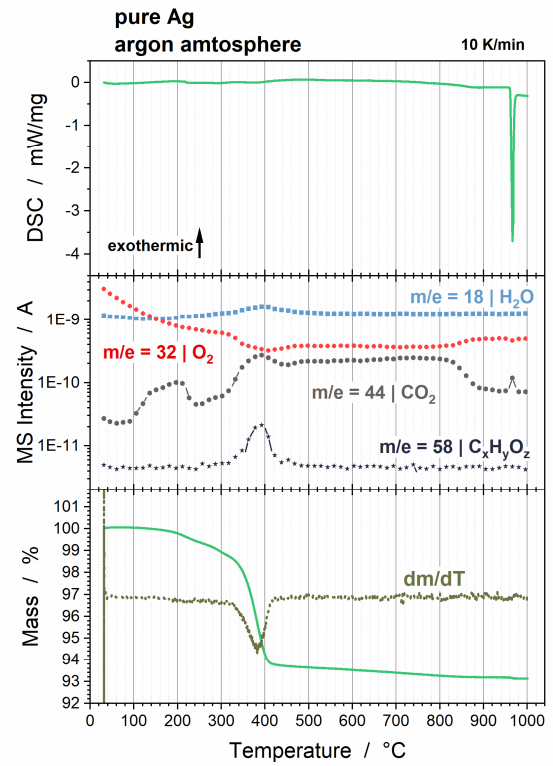

Fig. S7 DSC-TG and MS curves of pure Ag powder measured in argon atmosphere with 10 K/min.

References

1 H. M. Schadel and C. E. Birchenall, The vapor pressure of silver, *JOM*, 1950, **2**, 1134–1138.

2 M. Ohring, *Materials science of thin films. Deposition and structure*, Academic Press, San Diego, CA, 2nd edn., 2002.

3 R. A. Young, ed., *The Rietveld method*, Oxford Univ. Press, Oxford, 1995, vol. 5.

4 C. H. Macgillavry, G. D. Rieck and Lonsdale K., eds., *Physical and chemical tables*, Reidel, Dordrecht, 2nd edn., 1985, Vol. 3.

5 Nanografi, Ag(silver) Nanoparticles 48-78nm _ CAS.No: 7440-22-4 _ Safety Data Sheet, 2017.